Experimental Cell Research 343 (2016) 3–6

Contents lists available at ScienceDirect

Experimental Cell Research

journal homepage: www.elsevier.com/locate/yexcr

Review Article

Nanoscale and mechanical properties of the physiological cell–ECM microenvironment

Jennifer L. Young [a], Andrew W. Holle [a], Joachim P. Spatz [a,b,*]

[a] Department of New Materials and Biosystems, Max Planck Institute for Intelligent Systems, Stuttgart 70569, Germany
[b] Department of Biophysical Chemistry, University of Heidelberg, Heidelberg 69047, Germany

ARTICLE INFO

Article history:
Received 26 September 2015
Accepted 29 October 2015
Available online 30 October 2015

Keywords:
Extracellular matrix
Nanoscale
Stiffness
Topography
Ligands

ABSTRACT

Studying biological processes *in vitro* requires faithful and successful reconstitution of the *in vivo* extracellular matrix (ECM) microenvironment. However, the physiological basis behind *in vitro* studies is often forgotten or ignored. A number of diverse cell-ECM interactions have been characterized throughout the body and in disease, reflecting the heterogeneous nature of cell niches. Recently, a greater emphasis has been placed on characterizing both the chemical and physical characteristics of the ECM and subsequently mimicking these properties in the lab. Herein, we describe physiological measurement techniques and reported values for the three main physical aspects of the ECM: tissue stiffness, topography, and ligand presentation.

Contents

1. Tissue stiffness

Mechanical properties of the ECM have been shown to play integral roles in morphogenesis, development, and disease (Fig. 1). While the appreciation that cells should be cultured in or on substrates of physiological stiffness has been growing, most substrates have been modeled after *in vitro* measurements of tissues. Many different values of tissue stiffness can be obtained depending on measurement technique, analysis of generated data, or activity state of dynamic tissues; thus it remains important to determine the system that best represents the biological environment of interest. Additionally, there are inherent limitations in the direct *in vivo* measurement of each tissue system, as well as the scale of measurement, i.e. macro- *vs.* micro- *vs.* nano-scale analysis. To date, multiple measurement techniques have been employed to study mechanical properties of tissues, often focusing on determining the Young's, or elastic, modulus (E), expressed in Pascals (Pa). Due to the fact that *in vivo* mechanical properties have been shown to vary from those measured *in situ* or *in vitro* [1], we focus here only on *in vivo* experiments that can best recapitulate biological values.

In vivo measurement techniques have become increasingly important as a diagnostic tool for a variety of conditions due to their ability to non-invasively assess tissue architecture and physical properties, which are often altered in disease. Many tumors manifest as stiff masses, *e.g.* in breast scirrhous carcinoma, prostate cancer and thyroid cancer, while others are softer compared to healthy tissue, *e.g.* intraductal and papillary carcinoma [2]. Various imaging-based techniques have been employed to non-invasively measure the *in vivo* mechanical properties of soft tissues in patients based on ultrasound (US), optical coherence tomography

* Corresponding author at: Department of New Materials and Biosystems, Max Planck Institute for Intelligent Systems, Stuttgart 70569, Germany.
E-mail addresses: young@is.mpg.de (J.L. Young), holle@is.mpg.de (A.W. Holle), spatz@is.mpg.de (J.P. Spatz).

http://dx.doi.org/10.1016/j.yexcr.2015.10.037

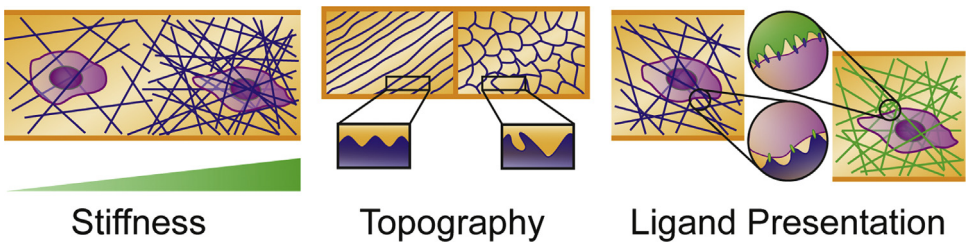

Fig. 1. Physiological cell–ECM interactions. Three main physiological matrix characteristics dominate cell–ECM interactions. ECM stiffness plays an important role in contractility-based mechanotransduction. ECM topography is dictated by the orientation of ECM fiber deposition. Ligand presentation also is influenced by ECM deposition, with an extra emphasis placed on the regular interval spacing of key cell binding ligands found in different proteins.

(OCT), and magnetic resonance elastography (MRE) [3].

Combining US with an OCT-based air-jet indentation system, stiffness of forefoot plantar soft tissue, an area prone to the development of foot lesions in the elderly, was non-invasively measured and shown to increase significantly with age, especially in the second metatarsal head, from $E\sim58.3$ kPa at ~27 years old to $E\sim83.2$ kPa at ~62 years old [4]. Similarly, studies on forearm mechanics determined the elastic modulus of skin to be ~210 kPa and adipose tissue ~1.9 kPa, both in the resting state [5]. Transient elastography has been used to correlate the extent of liver fibrosis and tissue stiffness, with an increase from $E\sim4.9$ kPa at F_0 to $E\sim25.3$ kPa at F_4 [6], reflecting the interconnected nature of ECM mechanics and disease progression. This connection is also seen in the brain, with stiffness decreasing with age and multiple sclerosis in a process termed "liquification". Using MRE, this observation was confirmed in a mouse model, with viscoelasticity decreasing from $|G^*|$ (complex shear modulus) ~10 kPa to $|G^*|$ ~8 kPa after 12 weeks [7].

US elastography has been used to describe the mechanical properties of numerous tissues, with varied results [3,8]. There are many confounding factors to be considered when examining *in vivo* US elastography data, but it can be reasonably concluded that the Young's modulus of parenchymal tissue is ~10 kPa, muscle is ~20 kPa and connective tissue is ~50 kPa [3]. Real-time shear wave elastography, a method based on US elastography, has also been utilized to more accurately measure tissue stiffness. Indeed, in a similar study of liver fibrosis, this technique reflects MRE-generated data, with stiffness at F_0 of $E\sim5.8$ kPa increasing to ~22.0 kPa at F_4 in a rabbit model [9].

At the cellular level, *in vivo* mechanics of the developing embryo have been examined using cell-sized oil microdroplets introduced between cells in a living tissue. Shape changes in these droplets can be utilized to calculate cell-generated local stresses, with the anisotropic stresses in the living dental mesenchyme of the mouse at embryonic stage E11 measured to be 1.6 ± 0.8 nN μm^{-2} [10]. Further analysis and application of this technique could provide a measure of the dynamic material properties of cells and/or tissues in a variety of organ systems.

When examining previous studies, it is apparent that measured values are highly dependent on numerous factors; thus, one must determine which set of conditions properly represents the relevant mechanical properties for a given experiment. It is also important to note that within tissues themselves, heterogeneous structures or dynamic states can exist which can also confound such mechanical measurements, *e.g.* cardiac muscle in systole is as high as $E\sim100$ kPa but drops to approximately 10 kPa in diastole [3].

2. Topography

Topographical effects on *in vitro* cell behavior have been explored in numerous systems. While a handful have included features inspired by tissue architecture, many lack a defined biological basis, as has been recently pointed out [11]. The lack of biomimicry in such studies is mostly a result of technical challenges and the lack of literature elucidating the exact topographical nature of the ECM *in vivo*.

In general, topographical features of the ECM include pore size, fiber diameter, and feature elevation (Fig. 1). Methods used to characterize the topography of physiological tissues almost always rely on tissue explants, a technique that can be problematic due to the possibility of topographical artifacts created by the fixation technique. The surface of these explants can be analyzed with transmission electron microscopy (TEM), scanning electron microscopy (SEM), and atomic force microscopy (AFM) to gain a more complete understanding, although the values reported by each of these techniques can vary within a single sample [12]. Due to the heterogeneous nature of tissues, it is no surprise that each tissue microenvironment presents a unique topographical fingerprint to the cells within it.

Several types of ECM exhibit mesh-like nanoscale structures, with fiber diameter and pore size dominating the topographical landscape [13]. The basement membrane, a ubiquitous ECM structure separating cell layers from interstitial ECM, is responsible for a number of tissue functions, including polarization and compartmentalization. Basement membranes extracted directly from macaque monkey corneas were found to have elevations of 150–190 nm, fiber diameters of 77 nm, and pore diameters of 72 nm [12], with general repetitive structures spaced on the order of 100 nm [14]. These features were also found in Matrigel, a commercially available basement membrane extract secreted by Engelbreth-Holm-Swarm mouse sarcoma cells [12], although Matrigel pore diameters are approximately 50% larger than those in native basement membrane tissue.

ECM fibers in the dermis have diameters of approximately 60–120 nm, with the diameter increasing with increased depth [15]. *In vivo* reflectance confocal microscopy has been used to analyze the topography of human skin in relation to its degree of sun exposure, revealing patterns in micron-scale keratinocyte layers. In general, more sun-exposed sites featured thicker and rougher stratum corneum and thinner stratum granulosum. This likely reflects changes in the cellular composition of these layers, but also reveals important alterations in the micron-scale physical ECM microenvironment of cancer-receptive zones [16]. Nanoscale anisotropy of skin ECM, likely arising from the macroscale Langer cleavage lines covering the body, may also contribute to skin-specific cell behavior [17]. In bone, collagen fibers have diameters between 80 and 100 nm, with small, 1–4 nm thick, 50×25 nm^2 carbonated apatite regions [18].

While some ECM environments are rather chaotic, others, including the myocardium and tendons, are highly organized. Ultrasound analysis of *ex vivo* rat myocardium revealed that the ECM contained fibers of approximately 100 nm diameter exhibiting strong directionality and alignment in parallel with the cell layer [11]. Ligaments and tendons have staggered collagen bundles with

diameters between 50 and 500 nm, all of which are incorporated into macroscale anisotropic fascicles and fibers with diameters as high as 500 μm [19]. It is important to note that the ECM is not the only source of ordered topographical information; cells themselves have been shown to be periodic and anisotropic. Muscle fibers are cylindrical multinucleated cells with diameters between 5 and 100 μm [20], in contrast to rectangular cardiomyocytes comprising patterned cardiac tissue with lengths between 100 and 150 μm and widths between 20 and 35 μm [21].

The design of natural and synthetic scaffolds for the study of cell–ECM interactions must continue to take *in vivo* observations of topography into account [22] by mimicking feature height, porosity, and fiber diameter [23] patterns on the nano- and microscale. While many investigations into nanoscale topography in synthetic systems have focused on altering parameters from infraphysiological to physiological to supraphysiological [24], the subtle changes in nanotopography from tissue to tissue should begin to be the focus of tissue-specific biomaterial design. Ultimately, patterns in topography influence cells not only in the physical structures presented to cells, but also in the presentation of spatially repeating cell-binding ligands along these protein fibers.

3. Ligand presentation

Many cells rely on the contacts they make with the ECM for survival and function (Fig. 1). Despite an increasing amount of work focusing on controlled ligand spacing in *in vitro* experiments, little is known about the precise presentation of ligands in the body. Due to resolution constraints of current imaging modalities and the limited availability of detection techniques, most information obtained about the cellular response to ligand orientation has been determined with *in vitro* experimentation by studying the response of cells to various synthetic substrates, leading to conclusions on the formation of focal contacts and actin cytoskeletal arrangements as a function of nanoscale control of cell-ECM contact [25,26]. Still, a handful of studies have shed light on biologically relevant ligand presentation with the use of protein structural analysis or novel imaging techniques.

Collagen is the most abundant protein in the body, and collagen fibers form bundles that interact at precisely defined interval spacing, termed D-spacing or periodicity [27]. This periodicity, while classically believed to be 67 nm [28,29], has been shown to be highly dependent on tissue type, with values ranging from ~63 to 72 nm [30]. While this periodicity contributes to nanoscale topography, it is also thought to be the scale at which cells can interact with ECM binding sites in healthy tissues. Indeed, this spacing has been confirmed *in vitro* for a variety of cell types, with peptide spacing over 73 nm leading to restricted integrin clustering [26].

Fibronectin (Fn) is another abundant protein in the ECM, and is essential for multiple homeostatic biological functions as well as pathological processes including fibrosis and cancer [31,32]. Early experiments using immunogold labeling of the alternatively-spliced domain A (situated between $FnIII_{11-12}$) in cellular fibronectin revealed a regular fibril arrangement in thick fibers (13–18 nm diameter) of approximately 42 nm, and in thin fibers (5–12 nm) of approximately 84 nm. The closer spacing in thicker fibers is thought to be due to the staggered alignment of fibrils [33], which could be further exacerbated in highly dense protein structures formed in aberrant processes like cancer [34]. Thus, the design of approaches to study the influence of the ECM in disease states must take these alterations in ligand spacing into account.

Crystal structure studies have provided a great deal of insight into the structural properties of single fibronectin fibrils [35], but fibrils exist in bundles in the body and thus alternative techniques have been developed to analyze these supramolecular structures. In recent studies, dSTORM imaging of fibronectin protofibrils allowed for the visualization of punctate IST-2 epitopes (which recognizes a site close to $FnIII_{12-14}$). Antibodies for N20 (N-terminus) and C20 (C-terminus) were also utilized, with each of these three antibodies separately exhibiting an average periodicity of ~95 nm [36]. Additionally, the average end-to-end distance of the fibers was determined to be ~133 nm, with an antiparallel overlap of 30–40 nm [36]. Such techniques could theoretically be used in combination with previous structural analyses to identify the precise presentation of each important cell-binding domain (present at FnI_5, $FnIII_{9-10}$, and alternatively spliced domain A between $FnIII_{11-12}$ and V between $FnIII_{14-15}$) within the fibronectin molecule [35].

While examination of single protein complexes is useful for parsing out their individual contributions, it is important to note that the ECM is comprised of a diverse set of proteins and adhesive molecules and that cells are constantly remodeling their extracellular matrix. For example, fibronectin intermingles with multiple molecules, including collagen, fibrin and heparin [35]. Ligand accessibility is likely very different between interacting proteins, not only in presentation, but also in which integrins are ligated. Therefore, changes in protein secretion and assembly will affect cellular behavior in the body, most importantly in dynamic processes like development or disease. Such variations in ligand presentation were demonstrated when heterotypic fibrils containing both fibronectin and type I collagen exhibited a periodicity of 67 nm *vs.* the 84 nm observed in fibronectin fibrils alone [33].

Exploring binding domains within protein assemblies is important in identifying all possible binding opportunities presented to a cell, but visualizing the contacts actually created by a cell could elucidate which adhesions contribute the most to its function. Indeed, it has been shown that intracellular variability exists between occupied and unoccupied receptors, suggesting that occupied ligands can dictate the physical distribution of integrin receptors [37]. Therefore, analyzing cytoskeletal components tightly linked to adhesion sites is an important yet challenging task. Actin/spectrin structures along neurons have been visualized with STORM super resolution microscopy, revealing evenly spaced ring-like structures along axonal shafts at a periodicity of 180–190 nm [38]. Other new techniques in cryo-electron tomography have allowed researchers to image focal adhesions in three dimensions within the cell. The complexes were found to have spacings of approximately 45 nm when plated on fibronectin-coated mesh grids [39]. Certainly, expanding these techniques to *in vivo* tissues would be an impressive and highly useful feat, as precise detection of cellular adhesions would provide valuable information for the design of *in vitro* cell scaffolds systems.

4. Conclusions

Numerous *in vitro* studies have shown that cells exhibit sensitivity down to the nanometer range, but often fail to correlate this sensitivity to physical parameters observed *in vivo*. Thus, novel approaches are needed to fully characterize the precise organization of physiological tissues, and then recreate such conditions *in vitro*. Intelligent design of synthetic and biological scaffolds should take values for ECM stiffness, topography, and ligand spacing into account, with special attention paid to the often small, yet crucial differences in these metrics between different cell niches. Furthermore, tissue dynamics must also be considered, as cells can reveal nanoscale cryptic epitopes in proteins as they exert force on their environment, making the physical signals a cell receives from its microenvironment highly variable [40,41].

Acknowledgments

The support from the Max Planck Society is highly appreciated. The article was assembled in the frame of the ERC Advanced grant (ERC Grant Agreement no. 294852) and the BMBF/MPG network MaxSynBio. J.P.S. is the Weston Visiting Professor at the Weizmann Institute of Science and is a member of the Heidelberg cluster of excellence CellNetworks.

References

[1] A. Gefen, S.S. Margulies, Are in vivo and in situ brain tissues mechanically similar? J. Biomech. 37 (2004) 1339–1352, http://dx.doi.org/10.1016/j.jbiomech.2003.12.032.
[2] I. Cespedes, J. Ophir, H. Ponnekanti, N. Maklad, Elastography: elasticity imaging using ultrasound with application to muscle and breast in vivo, Ultrason. Imaging 15 (1993) 73–88.
[3] P.N.T. Wells, H.-D. Liang, Medical ultrasound: imaging of soft tissue strain and elasticity, J. R. Soc. Interface 8 (2011) 1–29, http://dx.doi.org/10.1098/rsif.2011.0054.
[4] C.Y.L. Chao, Y.-P. Zheng, Y.-P. Huang, G.L.Y. Cheing, Biomechanical properties of the forefoot plantar soft tissue as measured by an optical coherence tomography-based air-jet indentation system and tissue ultrasound palpation system, Clin. Biomech. 25 (2010) 594–600, http://dx.doi.org/10.1016/j.clinbiomech.2010.03.008.
[5] J.T. Iivarinen, R.K. Korhonen, P. Julkunen, J.S. Jurvelin, Experimental and computational analysis of soft tissue stiffness in forearm using a manual indentation device, Med. Eng. Phys. 33 (2011) 1245–1253, http://dx.doi.org/10.1016/j.medengphy.2011.05.015.
[6] M. Yoneda, M. Yoneda, H. Mawatari, K. Fujita, H. Endo, H. Iida, et al., Noninvasive assessment of liver fibrosis by measurement of stiffness in patients with nonalcoholic fatty liver disease (NAFLD), Dig. Liver Dis. 40 (2008) 371–378, http://dx.doi.org/10.1016/j.dld.2007.10.019.
[7] K. Schregel, E. Wuerfel, P. Garteiser, I. Gemeinhardt, T. Prozorovski, O. Aktas, et al., Demyelination reduces brain parenchymal stiffness quantified in vivo by magnetic resonance elastography, Proc. Natl. Acad. Sci. U. S. A. 109 (2012) 6650–6655, http://dx.doi.org/10.1073/pnas.1200151109.
[8] K. Arda, N. Ciledag, E. Aktas, B.K. Arıbas, K. Köse, Quantitative Assessment of Normal Soft-Tissue Elasticity Using Shear-Wave Ultrasound Elastography, Am. J. Roentgenol. 197 (2011) 532–536, http://dx.doi.org/10.2214/AJR.10.5449.
[9] Y. Lu, J. Wei, Y. Tang, Y. Yuan, Y. Huang, Y. Zhang, et al., Evaluation of fatty liver fibrosis in rabbits using real-time shear wave elastography, Exp. Ther. Med. 8 (2014) 355–362, http://dx.doi.org/10.3892/etm.2014.1749.
[10] O. Campàs, T. Mammoto, S. Hasso, R.A. Sperling, D. O'Connell, A.G. Bischof, et al., Quantifying cell-generated mechanical forces within living embryonic tissues, Nat. Methods 11 (2013) 183–189, http://dx.doi.org/10.1038/nmeth.2761.
[11] D.-H. Kim, E.A. Lipke, P. Kim, R. Cheong, S. Thompson, M. Delannoy, et al., Nanoscale cues regulate the structure and function of macroscopic cardiac tissue constructs, Proc. Natl. Acad. Sci. U. S. A. 107 (2010) 565–570, http://dx.doi.org/10.1073/pnas.0906504107.
[12] G.A. Abrams, S.L. Goodman, P.F. Nealey, M. Franco, C.J. Murphy, Nanoscale topography of the basement membrane underlying the corneal epithelium of the rhesus macaque, Cell Tissue Res. 299 (1999) 39–46, http://dx.doi.org/10.1007/s004419900074.
[13] P. Martin, Wound healing–aiming for perfect skin regeneration, Science 276 (1997) 75–81, http://dx.doi.org/10.1126/science.276.5309.75.
[14] S. Goodman, Three-dimensional extracellular matrix textured biomaterials, Biomaterials 17 (1996) 2087–2095, http://dx.doi.org/10.1016/0142-9612(96)00016-6.
[15] A.S. Craig, E.F. Eikenberry, D.A.D. Parry, Ultrastructural organization of skin: classification on the basis of mechanical role, Connect. Tissue Res. 16 (2009) 213–223, http://dx.doi.org/10.3109/03008208709006977.
[16] M. Huzaira, F. Rius, M. Rajadhyaksha, R.R. Anderson, S. Gonzalez, Topographic variations in normal skin, as viewed by in vivo reflectance confocal microscopy, J. Investig. Dermatol. 116 (2001) 846–852, http://dx.doi.org/10.1046/j.0022-202x.2001.01337.x.
[17] R. Reihsner, B. Balogh, E.J. Menzel, Two-dimensional elastic properties of human skin in terms of an incremental model at the in vivo configuration, Med. Eng. Phys. 17 (1995) 304–313, http://dx.doi.org/10.1016/1350-4533(95)90856-7.
[18] S. Weiner, H.D. Wagner, The material bone: structure-mechanical function relations, Annu. Rev. Mater. Sci. 28 (1998) 271–298, http://dx.doi.org/10.1146/annurev.matsci.28.1.271.
[19] P. Fratzl, Cellulose and collagen: from fibres to tissues, Curr. Opin. Colloid Interface Sci. 8 (2003) 32–39, http://dx.doi.org/10.1016/S1359-0294(03)00011-6.
[20] J.J. Sciote, T.J. Morris, Skeletal muscle function and fibre types: the relationship between occlusal function and the phenotype of jaw-closing muscles in human, J. Orthod. 27 (2000) 15–30, http://dx.doi.org/10.1093/ortho/27.1.15.
[21] N.J. Severs, The cardiac muscle cell, BioEssays 22 (2000) 188–199, http://dx.doi.org/10.1002/(SICI)1521-1878(200002)22:2<188::AID-BIES10>3.0.CO;2-T.
[22] A.L. Bauer, T.L. Jackson, Y. Jiang, Topography of extracellular matrix mediates vascular morphogenesis and migration speeds in angiogenesis, Plos Comput. Biol. 5 (2009) e1000445, http://dx.doi.org/10.1371/journal.pcbi.1000445.
[23] M. Raoufi, T. Das, I. Schön, V. Vogel, D. Brüggemann, J.P. Spatz, Nanopore diameters tune strain in extruded fibronectin fibers, Nano Lett. 15 (2015) 6357–6364, http://dx.doi.org/10.1021/acs.nanolett.5b01356 (150911155515000).
[24] H.N. Kim, A. Jiao, N.S. Hwang, M.S. Kim, D.H. Kang, D.-H. Kim, et al., Nanotopography-guided tissue engineering and regenerative medicine, Adv. Drug Deliv. Rev. 65 (2013) 536–558, http://dx.doi.org/10.1016/j.addr.2012.07.014.
[25] S.P. Massia, J.A. hubbell, An RGD spacing of 440 nm is sufficient for integrin alpha V beta 3-mediated fibroblast spreading and 140 nm for focal contact and stress fiber formation, J. Cell Biol. 114 (1991) 1089–1100, http://dx.doi.org/10.1083/jcb.114.5.1089.
[26] M. Arnold, E.A. Cavalcanti-Adam, R. Glass, J. Blümmel, W. Eck, M. Kantlehner, et al., Activation of integrin function by nanopatterned adhesive interfaces, Chemphyschem 5 (2004) 383–388, http://dx.doi.org/10.1002/cphc.200301014.
[27] K. Gelse, Collagens—structure, function, and biosynthesis, Adv. Drug Deliv. Rev. 55 (2003) 1531–1546, http://dx.doi.org/10.1016/j.addr.2003.08.002.
[28] A.J. Hodge, J.A. Petruska, Recent studies with the electron microscope on ordered aggregates of the tropocollagen molecule, in: G.N. Ramachandran (Ed.), Aspects of Protein Structure, 1963, pp. 289–300.
[29] A.C. Lin, M.C. Goh, Investigating the ultrastructure of fibrous long spacing collagen by parallel atomic force and transmission electron microscopy, Proteins Struct. Funct. Genet. 49 (2002) 378–384.
[30] J.M. Wallace, Q. Chen, M. Fang, B. Erickson, B.G. Orr, M.M.B. Holl, I. Type, Collagen exists as a distribution of nanoscale morphologies in teeth, bones, and tendons, Langmuir 26 (2010) 7349–7354, http://dx.doi.org/10.1021/la100006a.
[31] W.S. To, K.S. Midwood, Plasma and cellular fibronectin: distinct and independent functions during tissue repair, Fibrogenesis Tissue Repair 4 (2011) 1–17.
[32] Y. Kyung Bae, A. Kim, M. Kyoung Kim, J. Eun Choi, S. Hwan Kang, S. Jung Lee, Fibronectin expression in carcinoma cells correlates with tumor aggressiveness and poor clinical outcome in patients with invasive breast cancer, Hum. Pathol. 44 (2013) 2028–2037, http://dx.doi.org/10.1016/j.humpath.2013.03.006.
[33] B.J. Dzamba, D.M. Peters, Arrangement of cellular fibronectin in non-collagenous fibrils in human fibroblast cultures, J. Cell Sci. 100 (Pt 3) (1991) 605–612.
[34] C.A. Sherman-Baust, A.T. Weeraratna, L.B.A. Rangel, E.S. Pizer, K.R. Cho, D. R. Schwartz, et al., Remodeling of the extracellular matrix through overexpression of collagen VI contributes to cisplatin resistance in ovarian cancer cells, Cancer Cell 3 (2003) 377–386, http://dx.doi.org/10.1016/S1535-6108(03)00058-8.
[35] M. Leiss, K. Beckmann, A. Girós, M. Costell, R. Fässler, The role of integrin binding sites in fibronectin matrix assembly in vivo, Curr. Opin. Cell Biol. 20 (2008) 502–507, http://dx.doi.org/10.1016/j.ceb.2008.06.001.
[36] S.M. Früh, I. Schoen, J. Ries, V. Vogel, Molecular architecture of native fibronectin fibrils, Nat. Commun. 6 (2015) 7275, http://dx.doi.org/10.1038/ncomms8275.
[37] S.E. LaFlamme, S.K. Akiyama, K.M. Yamada, Regulation of fibronectin receptor distribution, J. Cell Biol. 117 (1992) 437–447, http://dx.doi.org/10.1083/jcb.117.2.437.
[38] K. Xu, G. Zhong, X. Zhuang, Actin, spectrin and associated proteins form a periodic cytoskeletal structure in axons, Science 339 (2013) 452–456, http://dx.doi.org/10.1126/science.1232251.
[39] I. Patla, T. Volberg, N. Elad, V. Hirschfeld-Warneken, C. Grashoff, R. Fässler, et al., Dissecting the molecular architecture of integrin adhesion sites by cryo-electron tomography, Nat. Cell Biol. 12 (2010) 909–915, http://dx.doi.org/10.1038/ncb2095.
[40] C. Zhong, M. Chrzanowska-Wodnicka, J. Brown, A. Shaub, A.M. Belkin, K. Burridge, Rho-mediated contractility exposes a cryptic site in fibronectin and induces fibronectin matrix assembly, J. Cell Biol. 141 (1998) 539–551, http://dx.doi.org/10.1083/jcb.141.2.539.
[41] M.L. Smith, D. Gourdon, W.C. Little, K.E. Kubow, R.A. Eguiluz, S. Luna-Morris, et al., Force-induced unfolding of fibronectin in the extracellular matrix of living cells, Plos Biol. 5 (2007) 2243–2254, http://dx.doi.org/10.1371/journal.pbio.0050268, e268–2254.